MATERIALS SCIENCE

Rehealable, fully recyclable, and malleable electronic skin enabled by dynamic covalent thermoset nanocomposite

Zhanan Zou,[1]* Chengpu Zhu,[2]* Yan Li,[1] Xingfeng Lei,[2,3] Wei Zhang,[2†] Jianliang Xiao[1†]

Electronic skin (e-skin) mimicking functionalities and mechanical properties of natural skin can find broad applications. We report the first dynamic covalent thermoset-based e-skin, which is connected through robust covalent bonds, rendering the resulting devices good chemical and thermal stability at service condition. By doping the dynamic covalent thermoset with conductive silver nanoparticles, we demonstrate a robust yet rehealable, fully recyclable, and malleable e-skin. Tactile, temperature, flow, and humidity sensing capabilities are realized. The e-skin can be rehealed when it is damaged and can be fully recycled at room temperature, which has rarely, if at all, been demonstrated for e-skin. After rehealing or recycling, the e-skin regains mechanical and electrical properties comparable to the original e-skin. In addition, malleability enables the e-skin to permanently conform to complex, curved surfaces without introducing excessive interfacial stresses. These properties of the e-skin yield an economical and eco-friendly technology that can find broad applications in robotics, prosthetics, health care, and human-computer interface.

INTRODUCTION

As the largest organ in the human body, skin plays an important role in our daily interaction with the environment. Skin not only protects the internal tissues and organs but also provides sensation of temperature, pressure, vibration, and haptics (*1*, *2*). It has been of great interest to the research community to design and fabricate electronic skins (e-skins) with functionalities and mechanical properties comparable to natural skin because of their great potential in robotics, prosthetics, health care, and human-computer interface. Different sensing capabilities of e-skins have been realized by integrating tactile/pressure sensors (*3*), temperature sensors (*4*, *5*), strain sensors (*6*, *7*), humidity sensors (*6*, *8*), and chemical sensors (*9*). To obtain good compliance and conformability, design principles developed in flexible and stretchable electronics were introduced to create flexible and stretchable e-skins (*10*–*19*). Serpentine and mesh structures were adopted to achieve very high stretchability and softness comparable to natural skin (*4*–*6*, *18*). Off-the-shelf chips were successfully integrated with stretchable networks to realize high-performance, multifunctional e-skins with acquisition, filtering, amplification, and communication capabilities (*15*, *16*). Advanced materials—including single-crystal silicon, organic semiconductors, nanoparticles, nanowires, nanotubes, and graphene—were used to realize superior sensing performances of e-skins (*3*–*9*, *17*, *19*). Inspired by the wound healing capability of natural skin, rehealable e-skins have also been developed (*20*–*34*).

Here, we demonstrate a not only rehealable but also fully recyclable and malleable e-skin that can sense pressure, flow, temperature, and humidity. This e-skin is based on a newly developed dynamic covalent thermoset (polyimine) doped with silver nanoparticles (AgNPs). Compared with the other rehealable devices and electronics, our e-skin can be not only rehealed but also fully recycled and reprocessed because of the reversible bond exchange through simultaneous bond forming and breaking reactions under certain external stimuli (*35*, *36*). The recyclability of our e-skin can greatly reduce electronic waste and environmental impact and can also potentially decrease manufacturing cost. The malleability renders our e-skin the capability of changing into different configurations while keeping a stress-free state in the polymer network. This capability could avoid introducing excessive interfacial stresses when the e-skin is integrated with complex, irregular surfaces. Furthermore, the covalently bonded thermoset matrix used in this work ensures better mechanical strength and chemical stability of the e-skin at service condition than that of other approaches (*22*–*24*).These properties are distinct from conventional thermoset materials that cannot be reprocessed, reshaped, and recycled because of their highly cross-linked polymeric networks connected with irreversible covalent bonds. The prominent characteristics of the e-skin represent an economical and eco-friendly technology that can find wide applications in robotics, prosthetics, health monitoring, and biomedical devices.

RESULTS AND DISCUSSION

The rehealable and recyclable e-skin integrates tactile, flow, temperature, and humidity sensors, as conceptually shown in Fig. 1A. These sensors are fabricated using conductive polymers, obtained by doping a dynamic covalent thermoset, polyimine, with AgNPs. They are then integrated onto a polyimine substrate by heat pressing to ensure malleability, rehealability, and full recyclability of the entire e-skin. Covalent bonds are formed between the sensors and the substrate because of dynamic covalent bond exchange reactions at the interfaces. Serpentine interconnects are adopted to minimize the effects of strain on sensor performance when deformed. The e-skin can be easily conformed onto curved surfaces (for example, human arms and robotic hands) by applying moderate heat and pressure (Fig. 1A, left). The geometrical conformity of the e-skin is permanent because of its malleability, even after the pressure or force is removed (*35*, *37*). When moderately damaged (Fig. 1A, top center), the e-skin can be rehealed (Fig. 1A, right). The rehealed e-skin can restore mechanical and electrical properties comparable to the original device. When severe damage occurs or the device is never needed, the whole e-skin can be fully recycled, leaving no waste at all. Once recycled, short-oligomer/precursor solution and AgNPs

[1]Department of Mechanical Engineering, University of Colorado Boulder, Boulder, CO 80309, USA. [2]Department of Chemistry and Biochemistry, University of Colorado Boulder, Boulder, CO 80309, USA. [3]School of Materials Science and Engineering, Yunnan University, Kunming 650091, China.
*These authors contributed equally to this work.
†Corresponding author. Email: jianliang.xiao@colorado.edu (J.X.); wei.zhang@colorado.edu (W.Z.)

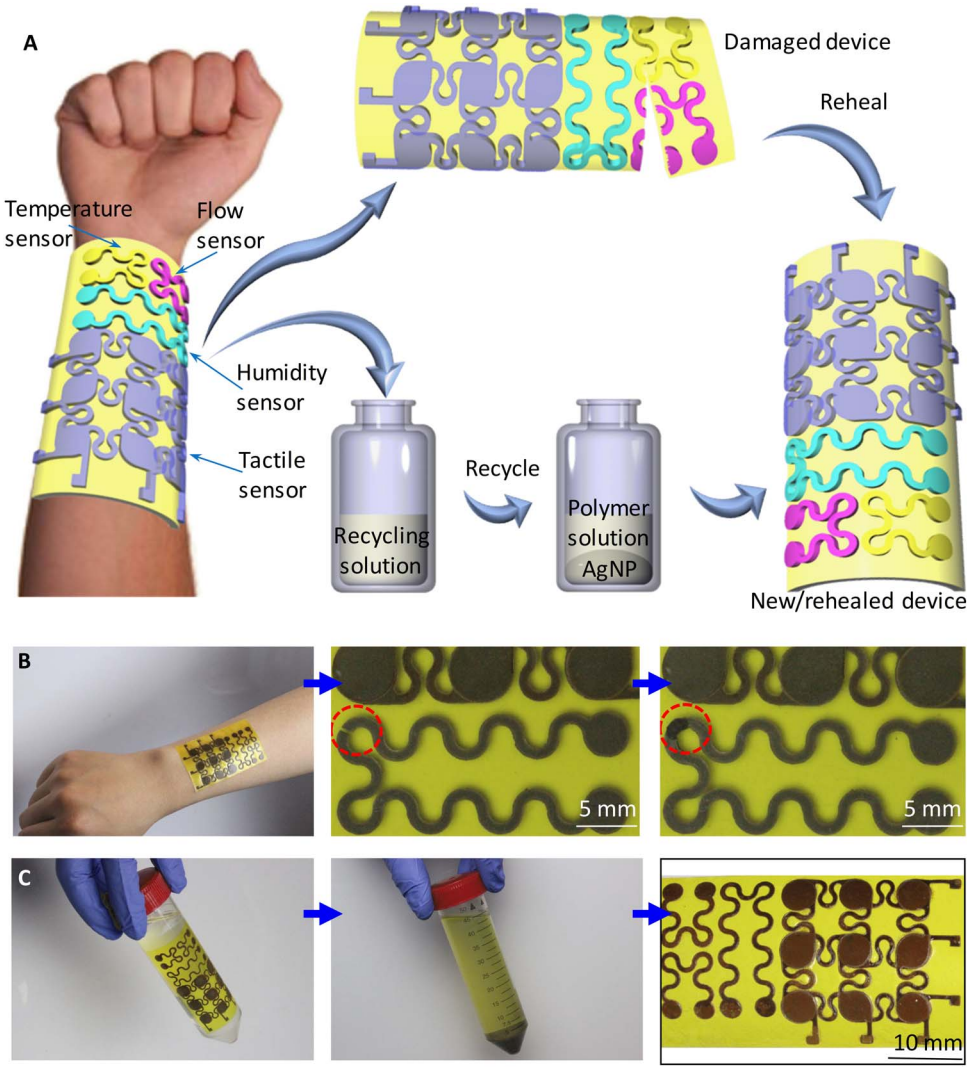

Fig. 1. Rehealable, fully recyclable, and malleable e-skin. (**A**) Schematic illustration of rehealability and full recyclability of the e-skin. (**B**) The malleable e-skin can be conformally mounted onto a human arm (left). When mechanically cut broken (middle), the e-skin can be rehealed by applying a small amount of rehealing agent and heat pressing (right). (**C**) The e-skin can be fully recycled using the recycling solution (left), yielding the solution with dissolved oligomers/monomers and AgNPs at the bottom (middle). The solution and AgNPs can be reused to make a new e-skin (right).

are obtained (Fig. 1A, bottom center) and can be used for making new materials and devices (Fig. 1A, right). Optical images in Fig. 1B illustrate the rehealing process of an e-skin. Because of the malleability provided by the polyimine substrate, the e-skin can be conformally mounted onto a human arm (Fig. 1B, left). When a sensor is broken because of mechanical cutting (Fig. 1B, middle), it completely loses its functionality. By applying a small amount of rehealing agent and heat pressing (8.5 kPa at 80°C), the broken sensor is rehealed, regaining its full sensing capability and mechanical integrity (Fig. 1B, right). To recycle the e-skin, simply soaking the whole device into the recycling solution (Fig. 1C, left) makes the polymer matrix degrade into oligomers and monomers that are soluble in ethanol (Fig.1C, middle), and the AgNPs sink to the bottom of the solution (bottom dark part). The recycled solution and nanoparticles are then used to make a new, functional e-skin (Fig.1C, right).

The polyimine film is prepared by mixing three commercially available compounds: (i) terephthalaldehyde (**1**), (ii) diethylenetriamine (**2**), and (iii) tris(2-aminoethyl)amine (**3**) in ethanol, as illustrated in Fig. 2A (see fig. S1 for the schematic illustration of a polyimine network). The detailed rehealing process of a pure polyimine polymer film is schematically illustrated in Fig. 2B, with optical images of the polyimine film shown at the bottom of each frame. A polyimine film (Fig. 2B, top left) is cut broken along its width direction (Fig. 2B, top right). By applying a small amount of rehealing solution (compounds **1**, **2**, and **3** in ethanol) at the cut area and by heat pressing (Fig. 2B, bottom right), the cut is rehealed (Fig. 2B, bottom left; see the Supplementary Materials for details). During rehealing, the new oligomers/polymers grow across the broken surfaces. This eventually leads to covalent (chemical) bonding of the two pieces, leaving no interfaces in the rehealed area, which mimics the natural skin rehealing process. This mechanism is different from traditional ways of bonding two material parts together, which rely on van der Waals (physical, noncovalent) interactions to form physical bonding at the interface. The interface remains after bonding, which usually leads to significant degradation in mechanical properties, such as elastic modulus and tensile strength. Figure 2C shows optical microscopy images of the cut at different stages of the rehealing process. The

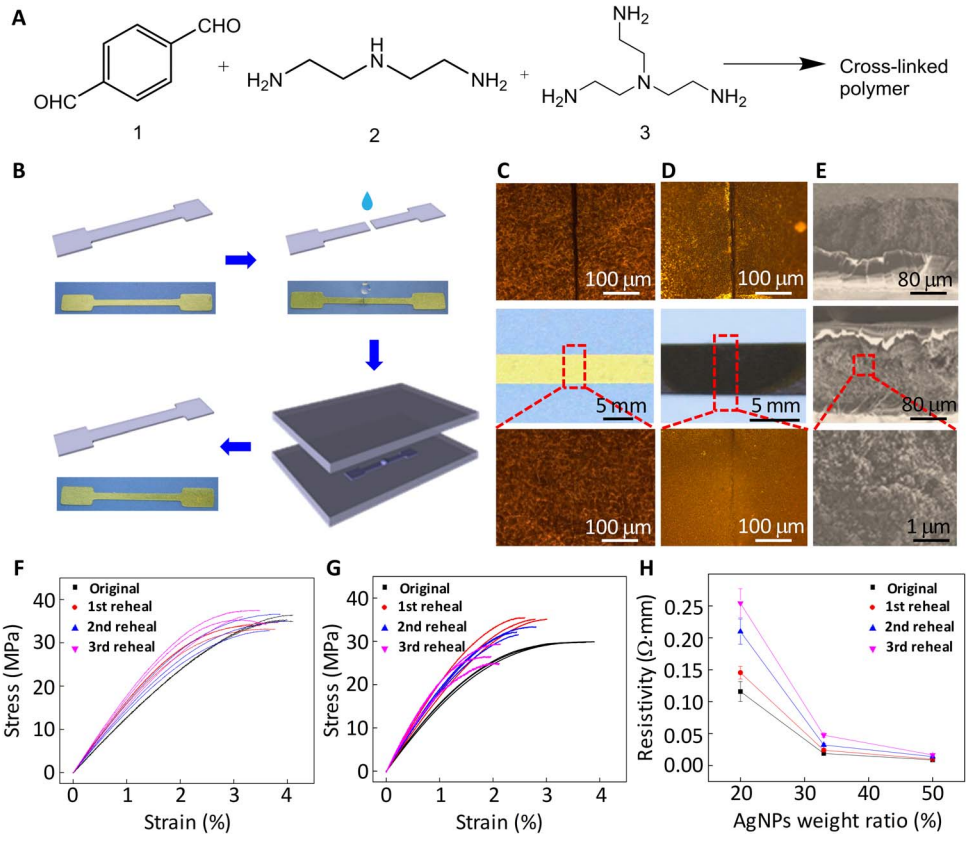

Fig. 2. Rehealing and characterization of the pure and conductive polyimine films. (**A**) Polymerization of the polyimine. (**B**) Schematic illustration of the rehealing process. Optical images of the polyimine film are shown at the bottom of each frame. (**C**) Optical microscopy images of a pure polyimine film that is cut broken (top) and rehealed (bottom). After rehealing, the cut is invisible (middle and bottom). (**D**) Optical microscopy images of a conductive polyimine film that is cut broken (top) and rehealed (bottom). After rehealing, the cut is invisible (middle), but traces of the cut can still be seen under microscope (bottom). (**E**) SEM images of the cross sections of a conductive polyimine film before (top) and after (middle) rehealing. The magnified view at the bottom shows the dispersion of AgNPs in the polymer network. Uniaxial tension test results of pure (**F**) and conductive (**G**) polyimine films before and after rehealing. Three samples were tested for each case. (**H**) Electrical resistivity measurements of the conductive polyimine films with different AgNP weight ratios before and after rehealing.

cut has a width of ~20 μm initially (Fig. 2C, top) and becomes invisible after it was rehealed, even under an optical microscope (Fig. 2C, middle and bottom). The conductive polyimine film, obtained by doping the dynamic covalent thermoset polyimine with AgNPs (particle size, ~100 nm; Sigma-Aldrich) at 33% weight ratio, can be rehealed through the same process as described in Fig. 2B, except that the rehealing agent consists of compounds **1**, **2**, and **3** and AgNPs in ethanol (see the Supplementary Materials for details). The top frame of Fig. 2D shows an optical microscopy image of a cut of width ~20 μm in a conductive polyimine film. After applying the rehealing agent and heat pressing, the cut is rehealed and becomes invisible (Fig. 2D, middle). Under the optical microscope, traces of the cut can still be seen (Fig. 2D, bottom), probably because the presence of AgNPs affects polymerization of monomers/oligomers. It is noteworthy that without any rehealing agent, both the pure polyimine and polyimine nanocomposite films can be rehealed under appropriate pressure and temperature conditions. Here, the introduction of a rehealing agent is to improve the healing effects, especially for polyimine nanocomposite films. Scanning electron microscopy (SEM) images of cross sections of the conductive polyimine before and after rehealing are shown in the top and middle frames of Fig. 2E, respectively. Good dispersion of AgNPs in the polymer network is shown in the magnified view (Fig. 2E, bottom).

A uniaxial tension test is conducted to compare the mechanical properties of pure and conductive polyimine films before and after rehealing. As shown in Fig. 2F, pure polyimine films restore their mechanical properties, such as elastic modulus, tensile strength, and maximum tensile strain, even after three times of rehealing. In addition, we observed that the locations of failure of the rehealed films were different from the previous failure points, indicating perfect rehealing effects. Figure 2G presents the uniaxial tension test results of conductive polyimine films (33% AgNP weight ratio) before and after rehealing. The elastic modulus and tensile strength are retained or even slightly increased. The average maximum tensile strain decreases by 23, 26, and 44% after the first, second, and third rehealing, probably because AgNPs complicate the interfacial bonding interactions, and multiple heat pressing treatments increase the brittleness of the films. Electrical resistivities of the conductive polyimine before and after rehealing are also investigated for three different AgNP weight ratios (20, 33, and 50%), as shown in Fig. 2H. After the first, second, and third rehealing, the electrical resistivity increases by 20% (27 and 13%), 44% (70 and 59%), and 119% (150 and 88%) for 25% (33 and 50%) AgNP weight ratio. In the following, conductive polyimine films with 33% AgNP weight ratio are used to fabricate sensors in the e-skin because of their good electrical property and mechanical robustness.

The recyclability of such polyimine and AgNPs material system is then explored. The stoichiometric balance between aldehyde and amine groups (their reaction forming the imine linkage) within the polyimine network can be upset by introducing an excess of free primary amine groups (for example, excess diamine monomer). Transimination reactions among the excess diamine monomers and the imine-linked network can lead to increased end groups within the matrix, thus reducing the molecular weight and solubilizing the network. Such a depolymerization mechanism could enable efficient recycling of the device consisting of dynamic covalent polyimine matrix and AgNPs. Figure 3A schematically illustrates the recycling process of a recyclable device. An old device is soaked in the recycling solution (ethanol and compound **2**) (top left) and decomposes into oligomers/monomers and AgNPs. The oligomers/monomers are soluble in the solution, and AgNPs sink to the bottom (top right). After recycling, the solution and AgNPs can be either separated or mixed together to make new materials or devices. To completely reuse the recycled solution and AgNPs to fabricate new devices, we proportionally added and efficiently mixed compounds **1** and **3** and additional AgNPs (bottom right). After polymerization, the conductive polyimine can be used to fabricate new devices (bottom left; see the Supplementary Materials for details). Figure 3B demonstrates the recycling of a conductive polyimine film. The light-emitting diode (LED) light turns on when the conductive polymer is integrated into a simple lighting circuit (top left). Then, the recycling solution is poured into a petri dish, causing decomposition of the polymer. After recycling is completed, the LED light turns off (top right). Subsequently, the solution and AgNPs are transferred out of the original circular petri dish and poured into a different, square petri dish (bottom right). Upon polymerization, the resulting film becomes conductive again and lights up the LED light (bottom left). The recycling processes can be completed within 6 hours at room temperature without sonication or within 2 hours with sonication and thus are very economical and eco-friendly (100% recyclable and reusable).

The stress-strain curves of pure polyimine films before and after recycling of up to three times are compared in Fig. 3C. The Young's modulus and tensile strengths of the recycled films increase by 20 and 26% compared with the original films, respectively. This could be due to the increased cross-linking density (more complete reaction) by using recycled oligomers as the starting materials instead of small-molecule–based monomers. Figure 3D exhibits the comparison of stress-strain curves of conductive polyimine films before and after recycling of up to three times. Similar increases in both Young's modulus and tensile strength are observed. Electrical resistivities of conductive polyimine films with 20, 33, and 50% AgNP weight ratios before and after recycling are compared in Fig. 3E. The results indicate that recycling does not show noticeable influence on electrical resistivity of the conductive polyimine films.

To demonstrate the great potential of these polyimine-AgNP nanocomposites toward e-skin applications, we next used the conductive polyimine films to fabricate tactile, flow, temperature, and humidity sensors, which are then integrated onto a polyimine substrate to form malleable, rehealable, and fully recyclable e-skin. The design of the e-skin is schematically illustrated in Fig. 4A, and an optical image of the e-skin is shown at the bottom. Serpentine structures are adopted to minimize the influence of strains on the performance of sensors. The tactile sensing is based on the capacitance change between two

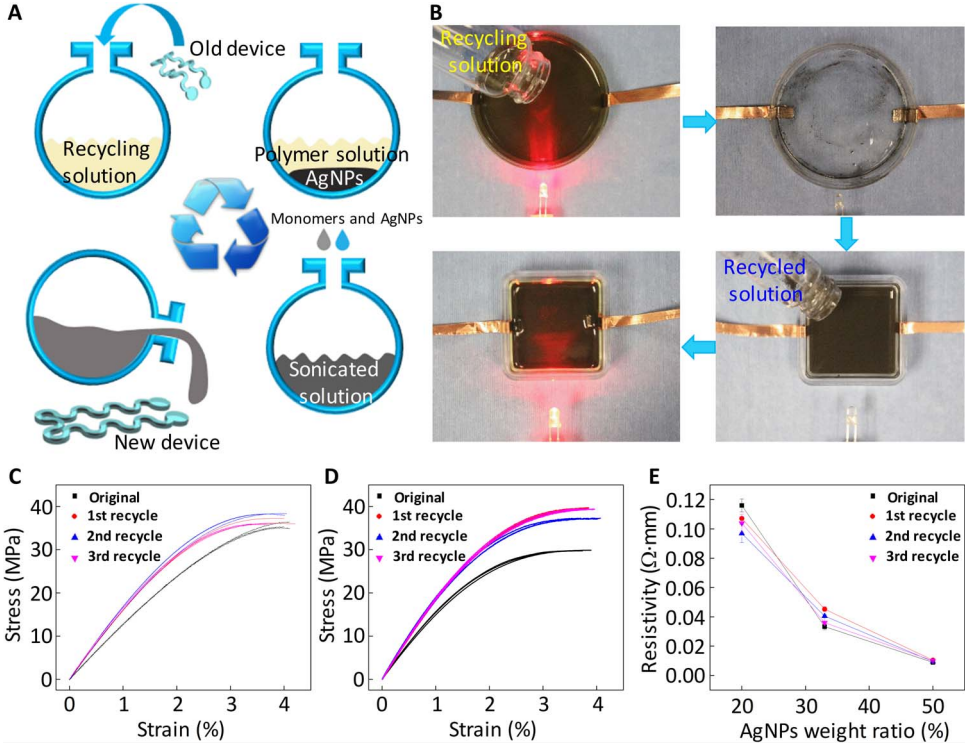

Fig. 3. Recycling and characterization of the pure and conductive polyimine films. (**A**) Schematic illustration of the recycling process. (**B**) The LED light is on when a conductive polyimine film is connected into a simple lighting circuit (top left). After recycling, the LED light turns off (top right). The recycled solution is then cast into a new, square petri dish (bottom right). After polymerization, the film is conductive and the LED light turns on (bottom left). Uniaxial tension test results of the pure (**C**) and conductive (**D**) polyimine films before and after recycling. (**E**) Electrical resistivity measurements of the conductive polyimine films before and after recycling.

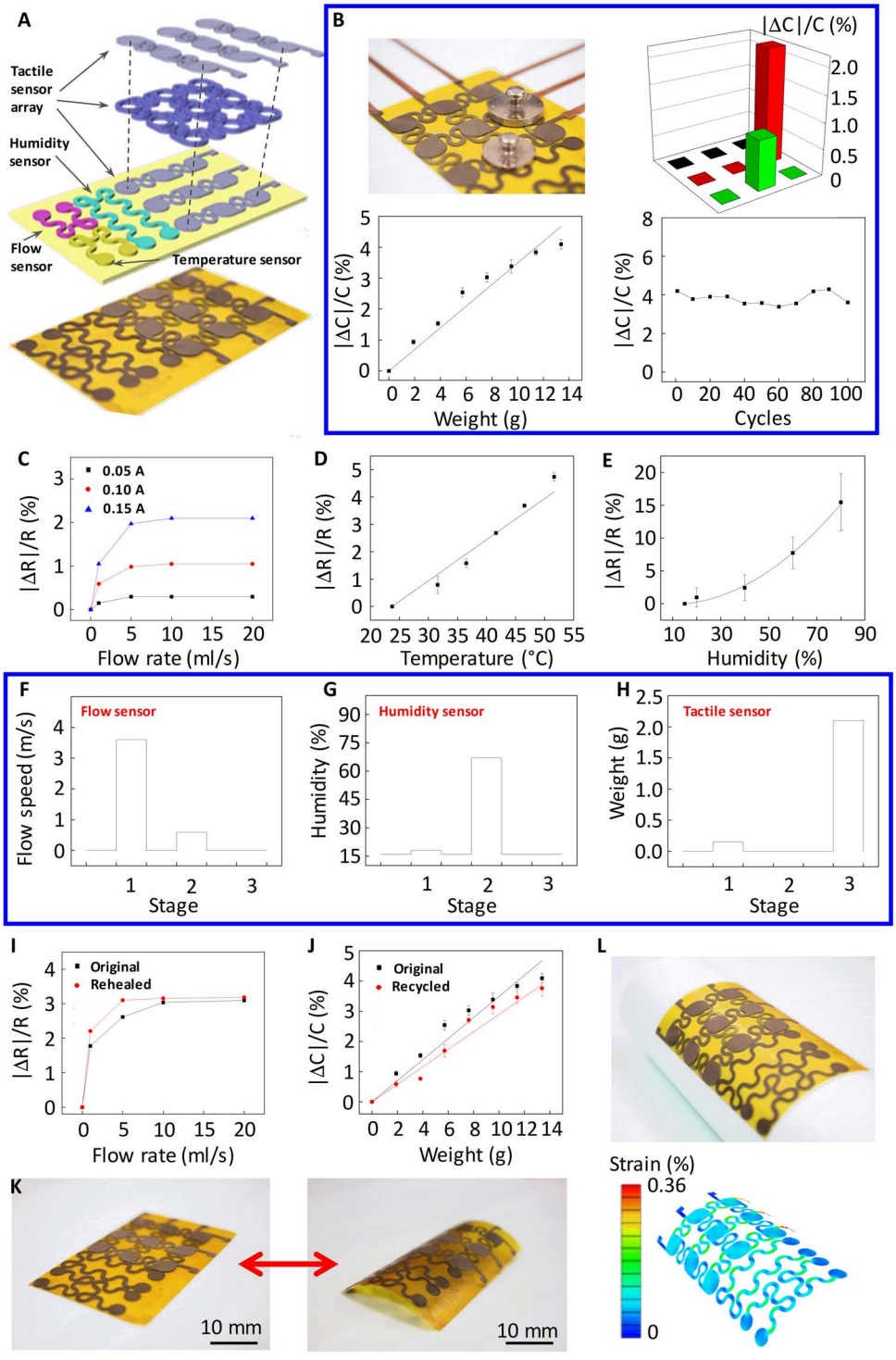

Fig. 4. Characterization of the rehealable, fully recyclable, and malleable e-skin. (**A**) Schematic illustration of the design of the e-skin (top). An optical image of the e-skin is shown at the bottom. (**B**) Characterization of the tactile sensor. When two different balance weights (2 and 5 g) are put on the top of the tactile sensor array (top left), both the weights and positions are detected (top right). The relative capacitance change of the tactile sensor versus weight shows a linear relationship (bottom left). Repeatability of the tactile sensor is tested for 100 cycles with a 13.2-g weight (bottom right). Characterization of the flow sensor with different currents (**C**), temperature sensor (**D**), and humidity sensor (**E**). The sensing performance of the flow sensor (**F**), humidity sensor (**G**), and tactile sensor (**H**) on an integrated e-skin in a complicated environment. Stages 1, 2, and 3 are corresponding to applying air flow, moisture, and screw nuts on the e-skin. (**I**) Comparison of sensing properties of the flow sensor before and after rehealing. (**J**) Comparison of sensing properties of the tactile sensor before and after recycling. (**K**) Malleability enables the e-skin to change its shape between flat (left) and curved (right) states. (**L**) Experimental image (top) and finite element analysis results (bottom) of the e-skin bended around a cylinder with a radius of 100 mm.

conductive element arrays (gray element arrays in Fig. 4A) separated by a dielectric polymer ring array (purple ring array in Fig. 4A). Figure 4B shows the performance of the tactile sensor. When two different balance weights (2 and 5 g) are placed on the tactile sensor array (top left), both the weights and positions are detected by the sensor (top right). The relative capacitance change versus weight shows linear relationship (bottom left). Loading and unloading of a 13.2-g weight is also tested 100 times to ensure repeatability (bottom right). Figure 4C exhibits the measured relative resistance change in the flow sensor versus flow rate at different currents. The measurement was conducted by controlling the water flow in a tube of 10 mm in diameter, and the flow sensor was attached on the inner wall of the tube. As shown in Fig. 4C, the flow sensor can sense flow rates lower than 10 ml/s, beyond which the flow sensor does not change its resistance with increasing flow rate anymore. As expected, increasing current can effectively enhance the sensitivity. Characterizations of the temperature sensor are presented in Fig. 4D. The sensor resistance changes linearly with temperature between 24° and 54°C. Humidity can be sensed on the basis of the plasticizing effect of water on polyimine. As water molecules diffuse into the sensor, the polymer network expands, leading to an increase of the sensor resistance. Figure 4E presents the measured relative resistance change of the humidity sensor versus humidity between 15 and 80%, which shows quadratic dependency. For details about the design, fabrication, and characterization of the sensors, see the Supplementary Materials.

The average sensitivities of the tactile, temperature, and humidity sensors can be obtained by calculating the average slopes of the curves in Fig. 4 (B, D, and E, respectively). The sensitivity of the tactile sensor is 0.0067 kPa^{-1}, which is comparable to most of the other reported sensitivities of e-skins (from 10^{-4} to 0.5 kPa^{-1}) (*38*). The sensitivity of the temperature sensor is 0.17%°C^{-1}, slightly smaller than that of the previously reported e-skin (<1%°C^{-1}) (*2*). The average sensitivity of the humidity sensor is 0.22%/%, which is higher than the other reported humidity sensors on e-skins (~0.08%/%) (*6*). The detection limits of the sensors are also indicated by the data shown in Fig. 4 (B to E). For each tactile sensor, the detection limit is between 0 and 14 g. Beyond 16 g, the deflection of the top conductive elements leads to their direct contact with the bottom elements and thus failure of tactile sensing. The flow sensor can detect water flow between 0 and 10 m/s. For the temperature sensor, the detection limit is below 60°C, above which the active bond exchange reactions in the polyimine network lead to large variation of the resistivity of the conductive polyimine. For the humidity sensor, the upper limit of detection is about 80 to 90%.

In addition to individual characterization, the sensing performance of the e-skin in a complicated environment combining air flow, humidity, and pressure was tested (see fig. S4 for more details). The results recorded by the flow, humidity, and tactile sensors are shown in Fig. 4 (F to H, respectively). The air flow and relative humidity of the ambient environment were 0 m/s and 15%, respectively, and there was no weight applied on the tactile sensors. At stage 1, constant air flow was applied on the surface of the e-skin (fig. S4A). The flow speed recorded by the flow sensor was 3.6 m/s (Fig. 4F), the humidity sensor also recorded an increase of 2% in humidity due to relatively more humid air flow than that of the environment (Fig. 4G), and the air pressure was also sensed by the tactile sensor, which was equivalent to 0.15 g (Fig. 4H). Afterward, the air flow was turned off, and the flow, humidity, and tactile sensors went back to the original states. At stage 2, a moisture generator was used to spray moisture on top of the e-skin (fig. S4B). The flow sensor recorded the flow speed to be 0.59 m/s (Fig. 4F), and the sensed relative humidity increased to 67% (Fig. 4G). Because the air pressure was very small, the tactile sensor did not give readable values (Fig. 4H). At stage 3, the moisture generator was turned off, and several screw nuts were placed on the top of the e-skin (fig. S4C). The central tactile sensor element gave the weight put on top of it to be 2.1 g (Fig. 4H), whereas the flow and humidity sensors did not show any changes (Fig. 4, F and G).

To demonstrate the rehealing capability of the e-skin, the flow sensor is cut broken and then rehealed using the process described previously. As shown in Fig. 4I, the rehealed flow sensor regains its flow sensing capability, which is comparable to the original sensor before cutting. Recycling of the tactile sensor is also demonstrated. Figure 4J compares the sensing characteristics of the tactile sensor in its original form and after recycling. The recycled tactile sensor shows similar sensing performance compared with the original tactile sensor. The slight reduction in sensitivity is probably due to the slight increase in Young's modulus of the recycled conductive polyimine film, as shown in Fig. 3D.

The e-skin is not only rehealable and recyclable but also flexible and malleable. By applying moderate heat (60°C), the flat e-skin (Fig. 4K, left) can be deformed into a curved shape. After cooling down and removing the applied force, the e-skin stays at its deformed, curved shape (Fig. 4K, right). This process is reversible and repeatable. Such property renders the e-skin excellent capability in matching with complex geometries, without incurring high stress buildup at the interface. Figure 4L shows that the e-skin is bended around a cylinder with a radius of 100 mm. Finite element simulation results provide the strain distribution in the deformed e-skin. The maximum strain in the deformed e-skin is 0.36%, much smaller than the failure strain of the conductive polyimine. The properties of the sensors under bending are also investigated. Figure S3 presents the sensing properties of the temperature, humidity, and tactile sensors when they are bent to a diameter of 100 mm, which show comparable behavior to these sensors in their flat states.

CONCLUSION

The e-skin based on polyimine and conductive AgNPs integrates tactile, flow, temperature, and humidity sensing capabilities and exhibits excellent rehealability, full recyclability, and malleability. The rehealed and recycled e-skin shows mechanical and electrical properties comparable to the original devices. Rehealing of the e-skin requires very moderate heating and pressure, and recycling only involves solution process at room temperature, which has rarely been reported for other e-skin systems. Both processes are very green and economical. Introducing these dynamic covalent polymers into a study on self-healable e-skin can bring both advantages of conventional thermosets (for example, high chemical/thermal stability and good mechanical property) and supramolecular polymers (for example, self-healing) into the development of the next-generation e-skins and wearable technology, with malleability, self-healability, and recyclability. Such technology has the potential to greatly reduce electronic waste that has caused severe pollution to the environment. Furthermore, the e-skin is robust yet flexible and malleable and thus can find applications in robotics, prosthetics, and biomedical devices. It is noteworthy that the formula of polyimine used in this work has relatively low stretchability and high strength. The reason of using the same polyimine as the supporting material was to achieve rehealability, full recyclability, and malleability of the entire

e-skin, including the sensing devices and the supporting substrate. However, the fabrication method can be slightly modified to integrate the conductive polyimine-based devices with soft substrates such as Ecoflex to achieve large stretchability and low effective modulus. Moreover, it is also possible to modify the imine chemistry to improve the stretchability of the polyimine network.

MATERIALS AND METHODS

Material preparation

The polyimine was synthesized by mixing terephthalaldehyde (compound **1**, 0.8 g; 5.96 mmol), diethylenetriamine (compound **2**, 0.184 g; 1.79 mmol), and tris(2-aminoethyl)amine (compound **3**, 0.407 g; 2.78 mmol) in ethanol. The solution was vigorously stirred and poured into a petri dish coated with polydimethylsiloxane (PDMS), followed by evaporating in a fume hood for 12 hours at room temperature and heat pressing at 80°C and 8.5 kPa. The conductive polyimine films were prepared by mixing the same compounds as described above and AgNPs in ethanol. The solution was sonicated for 2 hours and poured into a petri dish coated with PDMS, followed by evaporating in a fume hood for 12 hours at room temperature and heat pressing at 80°C and 8.5 kPa.

Rehealing and recycling process

To reheal both the pure and conductive polyimine films, we added a small amount of rehealing agent to the crack, followed by heat pressing at 80°C and 8.5 kPa. To recycle the pure and conductive polyimine films, we first added 1 equivalent diethylenetriamine (compound **2**, 0.046 g; 0.448 mmol) and 1 equivalent tris(2-aminoethyl)amine (compound **3**, 0.102 g; 0.685 mmol) to dissolve the polyimine film. Then, terephthalaldehyde (compound **1**, 0.2 g; 1.49 mmol) was added into the solution for polymerization. For conductive polyimine nanocomposites, extra AgNPs were added to adjust the weight ratio of the mixture.

Mechanical test

The mechanical tests were carried out using an Instron mechanical testing system. Testing samples were cut into dog-bone shapes with a laser cutter.

Fabrication and characterization of the sensors

The sensors were fabricated by cutting conductive polyimine films using a laser cutter (Lide laser-cutting machine). Four-point measurements were adopted to measure the resistance change of the temperature, flow, and humidity sensors. The tactile sensor was based on the capacitance change between two conductive polyimine disks separated by a pure polyimine ring. The conductive polyimine disks and pure polyimine ring were bonded together by heat pressing at 1 kPa and 80°C for 10 min. A capacitance meter (Excelvan M6013) was used to measure the capacitance change.

SUPPLEMENTARY MATERIALS

Supplementary material for this article is available at http://advances.sciencemag.org/cgi/content/full/4/2/eaaq0508/DC1

Supplementary Materials and Methods

Supplementary Text

fig. S1. Polymerization of polyimine networks.

fig. S2 Optical images of sensors.

fig. S3 Characterizations of sensors under bending and flat states.

fig. S4. Sensor characterization on integrated platform.

table S1. Resistance of the original conductive polyimine films.

table S2. Resistance of the conductive polyimine films after the first recycling.

table S3. Resistance of the conductive polyimine films after the second recycling.

table S4. Resistance of the conductive polyimine films after the third recycling.

Reference (*39*)

REFERENCES AND NOTES

1. V. E. Abraira, D. D. Ginty, The sensory neurons of touch. *Neuron* **79**, 618–639 (2013).
2. A. Chortos, J. Liu, Z. Bao, Pursuing prosthetic electronic skin. *Nat. Mater.* **15**, 937–950 (2016).
3. C. Wang, D. Hwang, Z. Yu, K. Takei, J. Park, T. Chen, B. Ma, A. Javey, User-interactive electronic skin for instantaneous pressure visualization. *Nat. Mater.* **12**, 899–904 (2013).
4. D.-H. Kim, N. Lu, R. Ma, Y.-S. Kim, R.-H. Kim, S. Wang, J. Wu, S. M. Won, H. Tao, A. Islam, K. J. Yu, T.-I. Kim, R. Chowdhury, M. Ying, L. Xu, M. Li, H.-J. Chung, H. Keum, M. McCormick, P. Liu, Y.-W. Zhang, F. G. Omenetto, Y. Huang, T. Coleman, J. A. Rogers, Epidermal electronics. *Science* **333**, 838–843 (2011).
5. D. Son, J. Lee, S. Qiao, R. Ghaffari, J. Kim, J. E. Lee, C. Song, S. J. Kim, D. J. Lee, S. W. Jun, S. Yang, M. Park, J. Shin, K. Do, M. Lee, K. Kang, C. S. Hwang, N. Lu, T. Hyeon, D.-H. Kim, Multifunctional wearable devices for diagnosis and therapy of movement disorders. *Nat. Nanotechnol.* **9**, 397–404 (2014).
6. J. Kim, M. Lee, H. J. Shim, R. Ghaffari, H. R. Cho, D. Son, Y. H. Jung, M. Soh, C. Choi, S. Jung, K. Chu, D. Jeon, S.-T. Lee, J. H. Kim, S. H. Choi, T. Hyeon, D.-H. Kim, Stretchable silicon nanoribbon electronics for skin prosthesis. *Nat. Commun.* **5**, 5747 (2014).
7. S. Lee, A. Reuveny, J. Reeder, S. Lee, H. Jin, Q. Liu, T. Yokota, T. Sekitani, T. Isoyama, Y. Abe, Z. Suo, T. Someya, A transparent bending-insensitive pressure sensor. *Nat. Nanotechnol.* **11**, 472–478 (2016).
8. D. H. Ho, Q. Sun, S. Y. Kim, J. T. Han, D. H. Kim, J. H. Cho, Stretchable and multimodal all graphene electronic skin. *Adv. Mater.* **28**, 2601–2608 (2016).
9. J. Kong, N. R. Franklin, C. Zhou, M. G. Chapline, S. Peng, K. Cho, H. Dai, Nanotube molecular wires as chemical sensors. *Science* **287**, 622–625 (2000).
10. D.-H. Kim, J. Xiao, J. Song, Y. Huang, J. A. Rogers, Stretchable, curvilinear electronics based on inorganic materials. *Adv. Mater.* **22**, 2108–2124 (2010).
11. D.-H. Kim, J. Song, W. M. Choi, H.-S. Kim, R.-H. Kim, Z. Liu, Y. Y. Huang, K.-C. Hwang, Y.-W. Zhang, J. A. Rogers, Materials and noncoplanar mesh designs for integrated circuits with linear elastic responses to extreme mechanical deformations. *Proc. Natl. Acad. Sci. U.S.A.* **105**, 18675–18680 (2008).
12. D.-H. Kim, J.-H. Ahn, W. M. Choi, H.-S. Kim, T.-H. Kim, J. Song, Y. Y. Huang, Z. Liu, C. Lu, J. A. Rogers, Stretchable and foldable silicon integrated circuits. *Science* **320**, 507–511 (2008).
13. Y. Wang, Z. W. Li, J. Xiao, Stretchable thin film materials: Fabrication, application, and mechanics. *J. Electron. Packag.* **138**, 020801 (2016).
14. Y. M. Song, Y. Xie, V. Malyarchuk, J. Xiao, I. Jung, K.-J. Choi, Z. Liu, H. Park, C. Lu, R.-H. Kim, R. Li, K. B. Crozier, Y. Huang, J. A. Rogers, Digital cameras with designs inspired by the arthropod eye. *Nature* **497**, 95–99 (2013).
15. S. Xu, Y. Zhang, L. Jia, K. E. Mathewson, K.-I. Jang, J. Kim, H. Fu, X. Huang, P. Chava, R. Wang, S. Bhole, L. Wang, Y. J. Na, Y. Guan, M. Flavin, Z. Han, Y. Huang, J. A. Rogers, Soft microfluidic assemblies of sensors, circuits, and radios for the skin. *Science* **344**, 70–74 (2014).
16. Y. Liu, J. J. Norton, R. Qazi, Z. Zou, K. R. Ammann, H. Liu, L. Yan, P. L. Tran, K.-I. Jang, J. W. Lee, D. Zhang, K. A. Kilian, S. H. Jung, T. Bretl, J. Xiao, M. J. Slepian, Y. Huang, J.-W. Jeong, J. A. Rogers, Epidermal mechano-acoustic sensing electronics for cardiovascular diagnostics and human-machine interfaces. *Sci. Adv.* **2**, e1601185 (2016).
17. H. Lee, T. K. Choi, Y. B. Lee, H. R. Cho, R. Ghaffari, L. Wang, H. J. Choi, T. D. Chung, N. Lu, T. Hyeon, S. H. Choi, D.-H. Kim, A graphene-based electrochemical device with thermoresponsive microneedles for diabetes monitoring and therapy. *Nat. Nanotechnol.* **11**, 566–572 (2016).
18. A. Miyamoto, S. Lee, N. F. Cooray, S. Lee, M. Mori, N. Matsuhisa, H. Jin, L. Yoda, T. Yokota, A. Itoh, M. Sekino, H. Kawasaki, T. Ebihara, M. Amagai, T. Someya, Inflammation-free, gas-permeable, lightweight, stretchable on-skin electronics with nanomeshes. *Nat. Nanotechnol.* **12**, 907–913 (2017).
19. T. Yokota, P. Zalar, M. Kaltenbrunner, H. Jinno, N. Matsuhisa, H. Kitanosako, Y. Tachibana, W. Yukita, M. Koizumi, T. Someya, Ultraflexible organic photonic skin. *Sci. Adv.* **2**, e1501856 (2016).
20. Y. Li, S. Chen, M. Wu, J. Sun, Polyelectrolyte multilayers impart healability to highly electrically conductive films. *Adv. Mater.* **24**, 4578–4582 (2012).
21. C. Wang, H. Wu, Z. Chen, M. T. McDowell, Y. Cui, Z. Bao, Self-healing chemistry enables the stable operation of silicon microparticle anodes for high-energy lithium-ion batteries. *Nat. Chem.* **5**, 1042–1048 (2013).
22. K. S. Toohey, N. R. Sottos, J. A. Lewis, J. S. Moore, S. R. White, Self-healing materials with microvascular networks. *Nat. Mater.* **6**, 581–585 (2007).
23. P. Cordier, F. Tournilhac, C. Soulie-Ziakovic, L. Leibler, Self-healing and thermoreversible rubber from supramolecular assembly. *Nature* **451**, 977–980 (2008).

24. B. C. Tee, C. Wang, R. Allen, Z. Bao, An electrically and mechanically self-healing composite with pressure- and flexion-sensitive properties for electronic skin applications. *Nat. Nanotechnol.* **7**, 825–832 (2012).
25. E. T. Thostenson, T.-W. Chou, Carbon nanotube networks: Sensing of distributed strain and damage for life prediction and self healing. *Adv. Mater.* **18**, 2837–2841 (2006).
26. Y.-L. Rao, A. Chortos, R. Pfattner, F. Lissel, Y.-C. Chiu, V. Feig, J. Xu, T. Kurosawa, X. Gu, C. Wang, M. He, J. W. Chung, Z. Bao, Stretchable self-healing polymeric dielectrics cross-linked through metal–ligand coordination. *J. Am. Chem. Soc.* **138**, 6020–6027 (2016).
27. J. Y. Oh, S. Rondeau-Gagne, Y.-C. Chiu, A. Chortos, F. Lissel, G.-J. N. Wang, B. C. Schroeder, T. Kurosawa, J. Lopez, T. Katsumata, J. Xu, C. Zhu, X. Gu, W.-G. Bae, Y. Kim, L. Jin, J. W. Chung, J. B.-H. Tok, Z. Bao, Intrinsically stretchable and healable semiconducting polymer for organic transistors. *Nature* **539**, 411–415 (2016).
28. C.-H. Li, C. Wang, C. Keplinger, J.-L. Zuo, L. Jin, Y. Sun, P. Zheng, Y. Cao, F. Lissel, C. Linder, X.-Z. You, Z. Bao, A highly stretchable autonomous self-healing elastomer. *Nat. Chem.* **8**, 618–624 (2016).
29. O. R. Cromwell, J. Chung, Z. Guan, Malleable and self-healing covalent polymer networks through tunable dynamic boronic ester bonds. *J. Am. Chem. Soc.* **137**, 6492–6495 (2015).
30. J. A. Neal, D. Mozhdehi, Z. Guan, Enhancing mechanical performance of a covalent self-healing material by sacrificial noncovalent bonds. *J. Am. Chem. Soc.* **137**, 4846–4850 (2015).
31. S. A. Odom, S. Chayanupatkul, B. J. Blaiszik, O. Zhao, A. C. Jackson, P. V. Braun, N. R. Sottos, S. R. White, J. S. Moore, A self-healing conductive ink. *Adv. Mater.* **24**, 2578–2581 (2012).
32. B. J. Blaiszik, S. L. Kramer, M. E. Grady, D. A. McIlroy, J. S. Moore, N. R. Sottos, S. R. White, Autonomic restoration of electrical conductivity. *Adv. Mater.* **24**, 398–401 (2012).
33. E. Palleau, S. Reece, S. C. Desai, M. E. Smith, M. D. Dickey, Self-healing stretchable wires for reconfigurable circuit wiring and 3D microfluidics. *Adv. Mater.* **25**, 1589–1592 (2013).
34. C. Hou, T. Huang, H. Wang, H. Yu, Q. Zhang, Y. Li, A strong and stretchable self-healing film with self-activated pressure sensitivity for potential artificial skin applications. *Sci. Rep.* **3**, 3138 (2013).
35. P. Taynton, K. Yu, R. K. Shoemaker, Y. Jin, H. J. Qi, W. Zhang, Heat- or water-driven malleability in a highly recyclable covalent network polymer. *Adv. Mater.* **26**, 3938–3942 (2014).
36. Y. Jin, Q. Wang, P. Taynton, W. Zhang, Dynamic covalent chemistry approaches toward macrocycles, molecular cages, and polymers. *Acc. Chem. Res.* **47**, 1575–1586 (2014).
37. P. Taynton, H. Ni, C. Zhu, K. Yu, S. Loob, Y. Jin, H. J. Qi, W. Zhang, Repairable woven carbon fiber composites with full recyclability enabled by malleable polyimine networks. *Adv. Mater.* **28**, 2904–2909 (2016).
38. S. C. Mannsfeld, B. C. Tee, R. M. Stoltenberg, C. V. Chen, S. Barman, B. V. Muir, A. N. Sokolov, C. Reese, Z. Bao, Highly sensitive flexible pressure sensors with microstructured rubber dielectric layers. *Nat. Mater.* **9**, 859–864 (2010).
39. I. Must, V. Vunder, F. Kaasik, I. Põldsalu, U. Johanson, A. Punning, A. Aabloo, Ionic liquid-based actuators working in air: The effect of ambient humidity. *Sens. Actuators B Chem.* **202**, 114–122 (2014).

Acknowledgments

Funding: Financial support from the NSF (grant no. CMMI-1405355) is gratefully acknowledged. **Author contributions:** Z.Z., C.Z., W.Z., and J.X. designed the experiments. Z.Z., C.Z., Y.L., and X.L. performed the experiments and analysis. Z.Z., C.Z., W.Z., and J.X. wrote the paper. **Competing interests:** J.X., W.Z., Z.Z., and C.Z. are inventors on a pending patent application filed through the U.S. Patent and Trademark Office (application no. 62/588,814, filed on 20 November 2017). Y.L. and X.L. declare that they have no competing interests. **Data and materials availability:** All data needed to evaluate the conclusions in the paper are present in the paper and/or the Supplementary Materials. Additional data related to this paper may be requested from the authors. Supplementary information accompanies this paper on www.advances.sciencemag.org/ index.html. Reprints and permissions information is available online at www.sciencemag.org/help/reprints-and-permissions.

Submitted 26 September 2017
Accepted 18 January 2018
Published 9 February 2018
10.1126/sciadv.aaq0508

Citation: Z. Zou, C. Zhu, Y. Li, X. Lei, W. Zhang, J. Xiao, Rehealable, fully recyclable, and malleable electronic skin enabled by dynamic covalent thermoset nanocomposite. *Sci. Adv.* **4**, eaaq0508 (2018).

Rehealable, fully recyclable, and malleable electronic skin enabled by dynamic covalent thermoset nanocomposite

Zhanan Zou, Chengpu Zhu, Yan Li, Xingfeng Lei, Wei Zhang and Jianliang Xiao

Sci Adv **4** (2), eaaq0508.
DOI: 10.1126/sciadv.aaq0508